Classification of Local Climate Zones Using ASTER and Landsat Data for High-Density Cities

Yong Xu, Chao Ren, Meng Cai, Ng Yan Yung Edward, and Tianjun Wu

Abstract—The local climate zone (LCZ) scheme provides a standard method to conduct urban heat island studies, in which urban landscapes are classified into different LCZs according to urban structures, land cover, and construction materials. Based on the LCZ classification scheme, the World Urban Database and Access Portal Tools (WUDAPT) is a new initiative to generate LCZ maps of cities worldwide with the use of freely available Landsat data. This paper aims to evaluate the performance of the original WUDAPT method in LCZ mapping for high-density cities. To further improve LCZ mapping accuracy for high-density cities, we investigate the usage of both freely available Landsat and advanced spaceborne thermal emission and reflection radiometer (ASTER) satellite data to generate better LCZ mapping results. Experiments on two high-density Chinese cities, Guangzhou and Wuhan, showed that combining Landsat and ASTER data can improve the overall performance of LCZ mapping results, especially for urban areas. This finding indicates that further applications of the WUDAPT method for high-density cities can include both ASTER and Landsat data.

Index Terms—Advanced spaceborne thermal emission and reflection radiometer (ASTER), high-density cities, Landsat, local climate zone (LCZ), remote sensing, urban areas.

I. INTRODUCTION

THE urban heat island (UHI) effect is regarded as one of the significant characteristics of urbanization, which is becoming more and more important as cities continue to expand in the 21st century [1], [2]. Although researchers around the world have conducted UHI studies, there had been no international standardized research approach for UHI studies until the local climate zone (LCZ) concept was developed [3]. The

LCZ system generates a climate-oriented classification of descriptive parameters, including not only a set of representative parameters to describe local urban morphology but also their association with a corresponding UHI effect [3]. Due to the standardized LCZ definition and classification hierarchy, this new system can be easily adopted in UHI studies and can also be used for cross-comparison of different UHI studies within and between cities.

The definition of LCZ is based on actual urban geographical data, for which buildings, street patterns, and land use and cover should be collected. However, in some cities, especially in some developing countries, updated urban structure data are not available. Satellite data have been exploited to collect urban structure data [4]–[6]. Based on the LCZ concept, a new initiative called the World Urban Database and Access Portal Tools (WUDAPT; http://www.wudapt.org) has been developed to generate LCZ maps and collect data on urban morphology worldwide [7], [8]. It aims to take advantage of freely available satellite imagery to classify urban landscapes into several categories according to a standardized LCZ classification scheme [9]. The WUDAPT product is not only suitable for urban climate studies, e.g., UHI assessments [3], it also has great potential for weather, climate, and air quality applications [10], [11].

Landsat data can achieve promising local climate mapping results for some European cities, whose urban morphology complies well with the standard LCZ definitions [9], [12]. However, one recent study [13] showed that the accuracy for LCZ mapping for Kyiv, Ukraine, is only about 64%, which might reflect that LCZ mapping results for some cities might not be as good as expected; this may also be true for some dense and highly compact Asian cities [14]–[16]. To get better results, efforts have been made to combine synthetic aperture radar (SAR) and Landsat data to achieve better mapping accuracy [12]. Nevertheless, preliminary testing results have indicated that addition of SAR textural data did not significantly improve the final LCZ mapping result, although the use of SAR data might be useful in directly deriving urban height information [12].

Advanced spaceborne thermal emission and reflection radiometer (ASTER) data have a higher spatial resolution than Landsat data and are now freely available. Thus, in this study, we aim to investigate the use of both ASTER and Landsat data to generate better LCZ mapping results for high-density Asian cities. Two large Chinese cities, Guangzhou and Wuhan, were chosen as case studies.

The reminder of this paper is organized as follows. In Section II, a review of LCZ is provided. A remote

sensing–based LCZ classification approach is introduced in Section III. Section IV shows case studies. The results for the two Chinese cities are given in Section V. Discussions and some conclusions are presented in Sections VI and VII.

II. REVIEW OF LCZ

UHI are one of the most important issues of urban climates. Previous urban climate studies have mainly focused on the extent and magnitude of UHI based on urban–rural classifications. A review study [17] showed that most of the previous urban climate studies lacked quantitative metadata of site exposure and land cover. Thus, the measurements, site descriptions, and assessments of UHI have no uniform standard or objective protocol as a basis for comparison, which affects the value of previous urban climate studies for practical usage [3]. In this situation, a novel urban land use classification was proposed [18] to guide UHI studies, and later, better urban morphology classification methods based on building shapes and materials and street configurations were further developed [19].

However, the above effects on urban land use classification still lacked a quantitative standard to define each category [3]. In 2012, a new urban structure classification system, the LCZ system, was developed to support urban climate studies [3]. In this system, urban structures are classified into 17 standard classes, including 10 urban classes and 7 natural classes (shown in Table I above). Each class was defined strictly with a set of standard parameters, including land use or cover, building construction and materials, and human activities, including anthropogenic heat, which can provide a standard method to conduct urban climate studies.

III. REMOTE SENSING–BASED LCZ CLASSIFICATION APPROACH
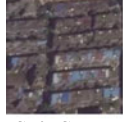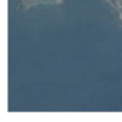
Because it is a fast and efficient means to provide land surface data for large areas, satellite technology has been extensively used in retrieving data on urban structures [4]–[6]. Based on the LCZ concept, WUDAPT was first proposed in 2012 to collect precise urban morphology data and activity data globally and to provide data suitable for climate science in a straightforward way and with free and open software and data [7], [9], [13].

A simple and straightforward LCZ mapping procedure using freely available Landsat data has been proposed [9]. The same procedure was revised for this study to include both Landsat and ASTER data as inputs. As shown below in Fig. 1, the improved LCZ classification approach has four main steps.

First, both Landsat and ASTER data in the study area were downloaded from the U.S. Geological Survey (USGS), preprocessed, and resampled at a resolution of 30 m. Both the spectral and textural features of the Landsat and ASTER data were used as input data.

Second, training areas for different LCZ types were selected via the Google Earth platform to ensure high quality. The selection principle was in accordance with the standard definition of each LCZ category.

TABLE I
STANDARD LCZ CLASSES [3], EXAMPLES FROM CHINESE CITIES

Third, based on the acquired Landsat and ASTER data and training areas, a random forest (RF) classification method was used to generate a local climate map.

Finally, the generated LCZ map with a spatial resolution of 30 m was resampled to 120 m according to the requirement of urban climate studies [9], [20]. An external independent test dataset was used to assess the overall accuracy (OA) of the generated local climate maps.

IV. CASE STUDY

A. Study Area

Two large cities in China were selected for our study: Guangzhou and Wuhan. Their locations are shown in Fig. 2. Guangzhou is the capital of Guangdong province in southern China. It is located in the northern part of the Pearl River Delta, facing the South China Sea, near Hong Kong and Macau. It has a permanent population of 13.5 million and covers an area of 7434 km^2. It is the largest city in southern China and the third largest in China. It has a subtropical monsoon climate and an annual average temperature of 20 to 22 °C.

Wuhan is the capital of Hubei province in central China. It has a population of 10 million and covers an area of 8494 km^2. The Yangtze and Hanjiang Rivers divide the city into three parts called Wuchang, Hankou, and Hanyang. Wuhan belongs to the

This article has been accepted for inclusion in a future issue of this journal. Content is final as presented, with the exception of pagination.

XU *et al.*: CLASSIFICATION OF LOCAL CLIMATE ZONES USING ASTER AND LANDSAT DATA FOR HIGH-DENSITY CITIES 3
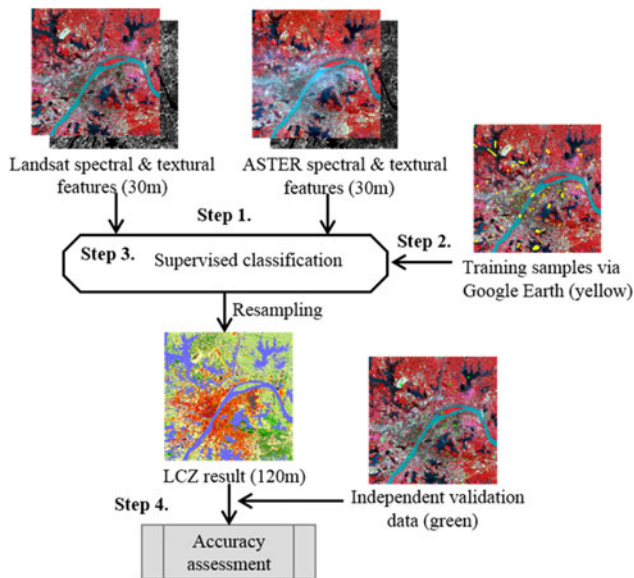
Fig. 1. Procedure of remote sensing–based LCZ classification approach.
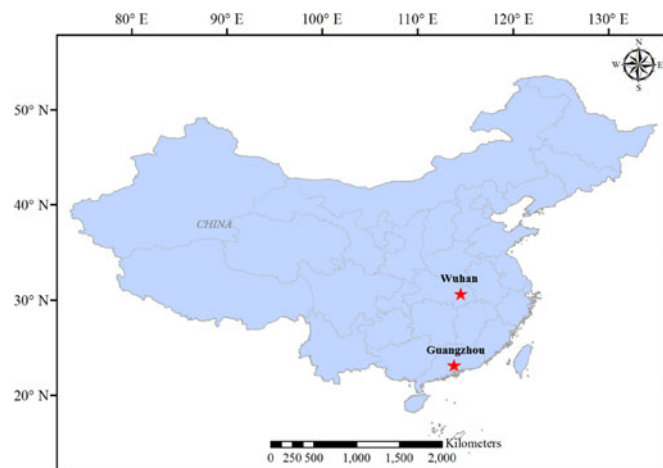
Fig. 2. Locations of Wuhan and Guangzhou in China.

Fig. 3. LCZ mapping results for Guangzhou using spectral and textural features from Landsat and ASTER data. (a) Satellite data, training areas (highlighted in yellow), and validation areas (highlighted in blue); (b) LCZ result.

Fig. 4. LCZ mapping results for Wuhan using spectral and textural features from Landsat and ASTER data. (a) Satellite data, training areas (highlighted in yellow), and validation areas (highlighted in blue); (b) LCZ result.

knowledge of the urban structures, which could benefit us in the selection of appropriate training and validation areas to conduct the study.

B. Input Data

Landsat and ASTER land surface reflectance data products for both Guangzhou and Wuhan were collected from the USGS. For Guangzhou, we used one Landsat image from 2014 (October 15, 2014) and two ASTER images from 2014 and 2016 (October 7, 2014, and July 8, 2016), and for Wuhan, we used one Landsat image from 2014 (October 6, 2014) and two ASTER images from 2013 (October 11, 2013). All acquired satellite data had undergone geometric correction. For the Guangzhou study area, the ASTER satellite data were projected onto the WGS84/UTM zone 49N coordinate system to ensure that the ASTER data were consistent with the coordinate system of the acquired Landsat data. For the Wuhan study area, both Landsat and ASTER data were projected onto the WGS84/UTM 50N coordinate system. After geometric correction, the ASTER images for both study areas were mosaicked into larger areas. The same area was then cropped from both datasets and used to test the proposed approach; Figs. 3(a) and 4(a) show the cropped areas with satellite data for both study areas of Guangzhou and Wuhan.

north subtropical monsoon zone, with hot summers and cold winters, high humidity, and poor overall comfort.

Due to their rapid urbanization and high population density, both cities suffer from hot summers with extremely high temperatures. In addition, they are prosperous and still undergoing rapid urbanization. Temperature studies for both cities have shown that the urban areas have significantly higher temperatures than the rural areas, indicating that they both experience an obvious UHI [21]–[25]. Hot weather and an intensified UHI worsen the thermal environment and pose a serious threat to their citizens' health.

These two cities were chosen for two other reasons. First, both cities are large, and high-density cities in China; Guangzhou, for example, is the third-largest city in China and has an extremely dense and compact urban morphology. Thus, both cities reflect the complexity of urban landscapes for large cities in China. Second, we are familiar with both cities and have local

This article has been accepted for inclusion in a future issue of this journal. Content is final as presented, with the exception of pagination.

4   IEEE JOURNAL OF SELECTED TOPICS IN APPLIED EARTH OBSERVATIONS AND REMOTE SENSING

TABLE II
FEATURE SETS, INCLUDING NAME, FEATURES USED, AND NUMBERS OF
FEATURES

Set name	Features	No.
AST	ASTER [Bands 1–3]	3
AST + GLCM	ASTER [Bands 1–3] + GLCM [Mean, Variance, Homogeneity, Contrast, Dissimilarity, Entropy, Second moment, Correlation]_PC1	11
LT8	Landsat 8 [Bands 1–7, 10–11]	9
LT8 + GLCM	Landsat 8 [Bands 1–7, 10–11] + GLCM [Mean, Variance, Homogeneity, Contrast, Dissimilarity, Entropy, Second moment, Correlation]_PC1	17
LT8 + AST	Landsat 8 [Bands 1–7,10–11]+ ASTER [Bands 1–3]	11
All	AST + GLCM, LT8 + GLCM	28

TABLE III
TRAINING AREAS FOR GUANGZHOU (GZ) AND WUHAN (WH)

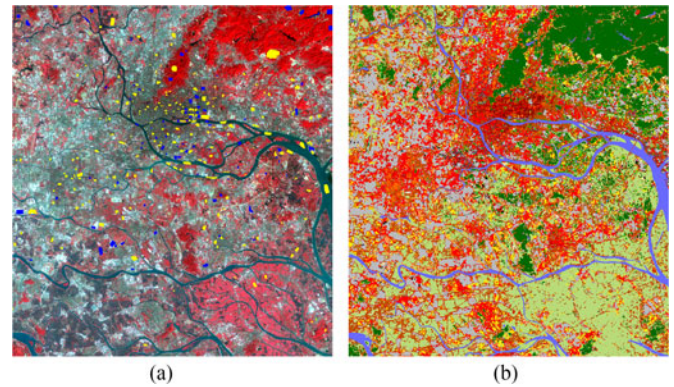|	Number of Training Areas		Number of Training Samples (30 m * 30 m)	
	GZ	WH	GZ	WH
LCZ1:Compact high-rise	14	23	1226	629
LCZ2: Compact mid-rise	27	18	1824	1412
LCZ3: Compact low-rise	20	20	2609	2533
LCZ4: Open high-rise	22	17	3779	2701
LCZ5: Open mid-rise	22	26	1700	3734
LCZ6: Open low-rise	10	13	1360	3030
LCZ7: Lightweight	10	10	1209	1521
LCZ8: Large low-rise	16	14	3246	2571
LCZ9: Sparse low-rise	6	8	311	347
LCZ10: Heavy industry	8	8	459	3729
LCZ A: Dense trees	10	9	4661	2726
LCZ B: Scattered trees	10	12	604	3049
LCZ C: Bush, scrub	8	8	477	728
LCZ D: Low plants	9	17	2966	7809
LCZ E: Bare rock or paved	9	12	312	1053
LCZ F: Bare soil or sand	5	14	267	3902
LCZ G: Water	10	15	3256	26 837

To provide a comprehensive understanding of both Landsat and ASTER data in generating the LCZ mapping result, both spectral and texture features from Landsat and ASTER data were used and compared. The spectral features included bands $1-7$ and $10-11$ of the Landsat 8 data and bands $1-3$ of the ASTER data. The textural features included eight gray-level co-occurrence textures (GLCM), representing mean, variance, homogeneity, contrast, dissimilarity, entropy, second moment, and correlation. The GLCM toolbox provided by commercial ENVI software was used generate all of the textural features on the basis of the first principal component of both Landsat and ASTER data. Given that the Landsat and ASTER data have a spatial resolution of 30 and 15 m, respectively, the used window sizes for calculating GLCM features for Landsat and ASTER data are $5*5$ and $7*7$, respectively.

As shown in Table II, six different combinations of features of Landsat or ASTER or both datasets were tested. The six testing feature sets included two sets based on multispectral features using either Landsat or ASTER data (LT8 and AST), two sets based on multispectral and texture information from either Landsat or ASTER data (LT8 + GLCM, AST + GLCM), one set based on the combined spectral information from both Landsat and ASTER data (LT8 + AST), and one set based on the combined spectral and texture information from both Landsat and ASTER data (All).

Moreover, the input of the proposed LCZ classification approach also included training areas, which were manually selected with Google Earth. Figs. 3(a) and 4(a) show the distribution of the selected training areas (highlighted in yellow) and validation areas (highlighted in blue), and Table III shows details of the training areas in both study areas, including the number of polygons and the number of pixel-based (30 m * 30 m) training samples per LCZ. For some LCZ classes, the number of training samples is small because the actual proportion of the corresponding class is rather small.

C. Classifiers

Three different classifiers were used to compare the performance of different feature sets in the generation of LCZ maps. The classifiers include multilayer perceptron neural network (NN), support vector machine (SVM), and RF.

The NN classifier is a feed-forward NN, in which standard back-propagation was used to train the weights of nodes in each layer. The nodes of the input layer correspond to the number of standard features, whereas the nodes of the output layer reflect the classification result. The nodes of hidden layers were empirically set as the mean nodes of the input and output layers. Each node of the network has an activation function to show its ability to transfer the information from input to output, which reflects that the responsibility of different nodes in processing different information and that all nodes work together to generate a final classification result.

The SVM classifier projects the original data into high-dimensional space to make them linearly separable. It is similar to the NN method, but instead, a kernel function was used to work as a hidden layer to separate the original data in a high-dimensional feature space. The output of SVM is the classification result.

The RF classifier can be considered as an extension of a conventional decision tree classifier. By reconstructing an ensemble of decision trees, a final classification result was conducted by integrating all results of different trees by voting. The RF classifier has good prediction accuracy and computation efficiency. Moreover, it can show the importance of input features by comparing different classification results with and without permuting features in a random way. Thus, the RF classifier implemented in open-source SAGA GIS software was used to conduct this study. As recommended in [12], the two parameters of RF, including the number of trees and the variable of the node, were given default values of 32 and the square root of the number of features for better memory management and computation efficiency of the SAGA software.

D. Performance Evaluation

To assess the prediction accuracy, independent validation data were manually selected via Google Earth, and double checked via Baidu 3D street map (www.baidu.com). Four quality indices,

This article has been accepted for inclusion in a future issue of this journal. Content is final as presented, with the exception of pagination.

XU *et al.*: CLASSIFICATION OF LOCAL CLIMATE ZONES USING ASTER AND LANDSAT DATA FOR HIGH-DENSITY CITIES

5

TABLE IV
VALIDATION AREAS FOR GUANGZHOU (GZ) AND WUHAN (WH)

	Number of Validation Areas		Number of Validation Samples (120 m * 120 m)	
	GZ	WH	GZ	WH
LCZ1:Compact high-rise	6	12	40	23
LCZ2:Compact mid-rise	5	7	24	38
LCZ3:Compact low-rise	7	6	39	34
LCZ4: Open high-rise	8	13	40	40
LCZ5: Open mid-rise	7	12	37	40
LCZ6: Open low-rise	5	4	33	40
LCZ7:Lightweight	6	7	16	40
LCZ8: Large low-rise	10	10	40	40
LCZ10: Heavy industry	3	3	40	40
LCZ A: Dense trees	6	3	40	40
LCZ B: Scattered trees	5	8	11	17
LCZ D: Low plants	5	6	40	40
LCZ E: Bare rock or paved	9	N/A	34	N/A
LCZ F: Bare soil or sand	N/A	8	N/A	40
LCZ G: Water	7	4	40	40

TABLE V
OA AND KAPPA INDICES OF LCZ MAPPING RESULTS USING DIFFERENT COMBINATIONS OF FEATURES WITH DIFFERENT APPROACHES AT GUANGZHOU STUDY AREA

Classifier	NN		RF		SVM	
Feature sets	OA	Kappa	OA	Kappa	OA	Kappa
AST	46	0.42	56	0.53	47	0.43
AST + GLCM	51	0.46	61	0.58	53	0.49
LT8	61	0.60	62	0.59	63	0.60
LT8 + GLCM	59	0.56	62	0.59	64	0.61
LT8 + AST	59	0.56	64	0.62	63	0.60
All	61	0.59	66	0.64	67	0.64

TABLE VI
OA AND KAPPA INDICES OF LCZ MAPPING RESULTS USING DIFFERENT COMBINATIONS OF FEATURES WITH DIFFERENT APPROACHES AT WUHAN STUDY AREA

Classifier	NN		RF		SVM	
Feature Sets	OA	Kappa	OA	Kappa	OA	Kappa
AST	31	0.26	66	0.63	50	0.46
AST + GLCM	55	0.51	71	0.69	64	0.61
LT8	70	0.67	81	0.79	77	0.75
LT8 + GLCM	72	0.69	81	0.79	77	0.75
LT8 + AST	72	0.69	82	0.80	80	0.78
All	77	0.75	84	0.83	84	0.83

including the OA, the user accuracy (UA), the producer accuracy (PA), and the kappa index, were used in this study. The OA reflects the OA of correction classification. UA refers to the proportion of correct classified pixels of a certain class divided by the predicted number of this class. PA refers to the proportion of correct classified pixels of a certain class divided by the total number of corresponding reference classes. The kappa index summarizes all different prediction errors into a single index. By comparing the generated LCZ map with the validation samples, a confusion matrix can be calculated, based upon which all indices can be obtained. Table IV shows the number of validation areas and the number of validation samples with the scale of the final LCZ map (120 m * 120 m). To reduce the flaws of standard kappa in interpretation [26], the number of validation samples for different classes were kept at the same level, except for a few classes that did not have enough validation samples.

V. RESULTS

A. LCZ Mapping Results of Guangzhou and Wuhan

For comparison, the accuracy of the LCZ mapping results with three classifiers and six feature sets were given. Tables V and VI show the OA and kappa indices for all results in both Guangzhou and Wuhan study areas; from these tables, we can see that the use of all spectral and textural features using both Landsat and ASTER data (All) achieved the best result, regardless of which classifier is adopted. RF and SVM both performed slightly better than the NN approach when both datasets were used, which indicates that both RF and SVM can be used for LCZ mapping tasks when multisource satellite data were used. The RF classifier is fast and efficient in generating LCZ maps, so it was used in this study to conduct LCZ mapping. Unless otherwise specified, the RF classifier was used in the remainder of this paper.

Based on the RF method, Fig. 3(b) shows the LCZ mapping result for Guangzhou, based on the spectral and textural information from both Landsat and ASTER data. It is apparent that the center of Guangzhou, in the northern part of the image (marked in red), is well classified as compact building settlements (LCZs 1–3). Except for the Guangzhou city center, some clusters with red color can be seen in the south and southwest of Guangzhou, which represent several satellite cities, such as Foshan and Shunde. Other than LCZs 1–3, some open building settlements marked in orange (LCZs 4–6) are located in the suburbs of each city. In addition, some large low-rise buildings with light colors can be seen in the middle of several cities. Although some samples that reflect heavy factory and sparse buildings are collected and used in this study, few locations are correctly classified into these two categories. Other than the area with urban types, most of the remaining areas are classified as low plants (LCZ D) and dense trees (LCZ A), highlighted in light green and dark green, respectively. This distribution is consistent with the actual land cover distribution as viewed with high-resolution imagery from Google Earth.

Fig. 4(b) shows the LCZ mapping result for Wuhan, based on spectral and textural information from both Landsat and ASTER data using the RF classifier. Compared with Guangzhou, Wuhan has fewer compact building settlements, as the majority of the center of Wuhan was classified as open buildings (LCZs 4–6) and only part of center area was classified as high-compact buildings (LCZs 1–3). In the suburbs of Wuhan, some large low-rise buildings with a light gray color and some sparsely distributed lightweight low-rise buildings with a yellow color can be seen. Other than urban classes (LCZs 1–10), most of the natural classes (LCZs A–F) in Wuhan are classified as low plants, with few areas of dense trees. Wuhan has less dense trees than Guangzhou.

This article has been accepted for inclusion in a future issue of this journal. Content is final as presented, with the exception of pagination.

6   IEEE JOURNAL OF SELECTED TOPICS IN APPLIED EARTH OBSERVATIONS AND REMOTE SENSING

TABLE VII
CONFUSION MATRIX FOR GUANGZHOU LCZ MAPPING RESULT USING LANDSAT AND ASTER DATA (ALL)

	1	2	3	4	5	6	7	8	10	A	B	D	E	G	Σref	PA
1	22	0	0	18	0	0	0	0	0	0	0	0	0	0	40	.55
2	0	12	3	0	9	0	0	0	0	0	0	0	0	0	24	.50
3	0	0	33	0	0	1	5	0	0	0	0	0	0	0	39	.84
4	9	0	2	18	11	0	0	0	0	0	0	0	0	0	40	.45
5	0	8	0	10	17	0	0	0	0	0	2	0	0	0	37	.46
6	0	0	0	2	3	11	7	1	0	0	1	7	1	0	33	.33
7	0	0	0	0	0	2	14	0	0	0	0	0	0	0	16	.87
8	0	0	1	0	0	0	0	39	0	0	0	0	0	0	40	.97
10	0	1	4	0	0	0	0	7	26	0	2	0	0	0	40	.65
A	0	0	0	0	0	0	0	0	0	40	0	0	0	0	40	1.0
B	0	0	0	0	0	0	0	0	0	0	5	6	0	0	11	.45
D	0	0	0	0	0	4	0	0	0	1	3	32	0	0	40	.80
E	0	15	1	1	5	0	0	6	0	0	0	0	6	0	34	.18
G	0	0	0	0	0	0	0	0	0	0	0	0	0	40	40	1.0
Σclass	31	46	44	49	45	18	26	53	26	41	13	45	7	40	Kappa:	0.64
UA	.71	.33	.75	.37	.38	.61	.54	.74	1.0	.98	.38	.71	.85	1.0	OA(%):	66

TABLE VIII
CONFUSION MATRIX FOR WUHAN LCZ MAPPING RESULT USING LANDSAT AND ASTER DATA (ALL)

	1	2	3	4	5	6	7	8	10	A	B	D	F	G	Σref	PA
1	16	1	0	2	2	0	0	0	2	0	0	0	0	0	23	.70
2	0	17	0	0	17	0	0	0	4	0	0	0	0	0	38	.45
3	0	0	30	0	0	0	3	0	0	0	0	0	1	0	34	.88
4	0	0	0	40	0	0	0	0	0	0	0	0	0	0	40	1.0
5	0	2	0	0	38	0	0	0	0	0	0	0	0	0	40	.95
6	0	0	0	3	7	26	3	0	0	0	0	1	0	0	40	.65
7	0	0	3	0	0	1	31	0	0	0	0	5	0	0	40	.78
8	0	0	2	0	0	0	0	34	2	0	0	0	2	0	40	.85
10	0	0	1	0	0	0	0	0	39	0	0	0	0	0	40	.98
A	0	0	0	0	0	0	0	0	0	35	5	0	0	0	40	.88
B	0	0	0	1	0	0	0	0	0	4	11	0	1	0	17	.65
D	0	0	0	0	0	0	0	0	0	0	2	38	0	0	40	.95
F	0	0	0	0	0	1	0	1	1	0	0	1	36	0	40	.90
G	0	0	0	0	0	0	0	0	0	0	0	0	0	40	40	1.0
Σclass	16	20	36	46	64	28	37	35	48	39	18	45	40	40	Kappa:	0.83
UA	1.0	.85	.83	.87	.59	.93	.84	.97	0.81	.90	.61	.84	.90	1.0	OA(%):	84

TABLE IX
ACCURACY STATISTICS FOR GUANGZHOU LCZ MAPPING RESULTS USING DIFFERENT FEATURES FROM EITHER LANDSAT OR ASTER OR BOTH DATASETS

Feature set	Natural Types (LCZs A-F)		Urban Types (LCZs 1-10)		All LCZs	
	OA (%)	Kappa	OA (%)	Kappa	OA (%)	Kappa
AST	90	0.87	52	0.45	56	0.53
AST + GLCM	81	0.75	56	0.50	61	0.58
LT8	94	0.92	61	0.55	62	0.59
LT8 + GLCM	92	0.89	61	0.56	62	0.59
LT8 + AST	92	0.89	64	0.59	64	0.62
All	93	0.90	65	0.60	**66**	**0.64**

TABLE X
ACCURACY STATISTICS FOR WUHAN LCZ MAPPING RESULTS USING DIFFERENT FEATURES FROM EITHER LANDSAT OR ASTER OR BOTH DATASETS

Feature set	Natural Types (LCZs A-F)		Urban Types (LCZs 1–10)		All LCZs	
	OA (%)	Kappa	OA (%)	Kappa	OA (%)	Kappa
AST	87	0.84	64	0.59	66	0.63
AST + GLCM	86	0.82	72	0.69	71	0.69
LT8	88	0.85	81	0.78	81	0.79
LT8 + GLCM	89	0.88	80	0.77	81	0.79
LT8 + AST	91	0.89	81	0.79	82	0.80
All	92	0.90	83	0.81	**84**	**0.83**

Guangzhou is much denser than Wuhan, which caused large prediction errors for urban types. With the generated LCZs, for example, Guangzhou had poor LCZ prediction results for urban types; the PA for LCZs 4–6 for Guangzhou were 45%, 46%, and 33%, respectively, and the same indices for Wuhan were 100%, 95%, and 65%, respectively.

In addition to the validation with independent testing data, training data were also used to validate the modeling accuracy using the RF classification method. The testing results show that both cities have extremely high modeling accuracy, with an OA of 0.98 for Guangzhou and 0.99 for Wuhan, which indicates that the prediction errors for both cities were mainly caused by the use of satellite data instead of the model.

VI. DISCUSSIONS

A. Advantages of Proposed Approach

The OA and kappa indices for the results based on the RF classifier using different sets of features are provided in Tables IX and X. To better compare the performance of different features in generating LCZ types with more details, the results for two major LCZ categories, including urban types (LCZs 1–10) and natural types (LCZs A–F), are also given.

Table IX shows the OA and kappa indices for all results for Guangzhou based on different features using Landsat and ASTER data. Columns 2 and 3 give the accuracy statistics for natural landscapes, and columns 4 and 5 show the accuracy statistics for urban types; the OA and kappa coefficients for all LCZ types are provided in columns 6 and 7. Similarly, the

B. Accuracy and Performance Analysis

Two indices, the OA and the kappa coefficient, were used to assess the final LCZ mapping results by comparing them with actual independent validation data. Table VII shows the validated results for Guangzhou, for which an OA of 66% was obtained with a kappa coefficient of 0.64. When we looked at the producer and UA for the results for Guangzhou, it was found that urban types had a relatively lower accuracy than natural types. For example, LCZ 1 for Guangzhou had a low PA of 0.55, whereas LCZ A, which reflects dense trees, has a high PA of 100%.

Table VIII gives the validation results for Wuhan, for which an OA of 84% and a kappa coefficient of 0.83 were obtained. The main reason for the higher accuracy than Guangzhou is that

This article has been accepted for inclusion in a future issue of this journal. Content is final as presented, with the exception of pagination.

XU *et al.*: CLASSIFICATION OF LOCAL CLIMATE ZONES USING ASTER AND LANDSAT DATA FOR HIGH-DENSITY CITIES
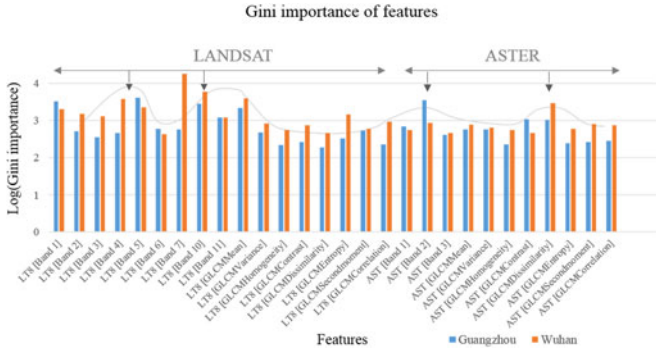7

Fig. 5. Gini importance of features from both Landsat and ASTER data.

accuracy statistics for the LCZ results of Wuhan are provided in Table X.

Based on the accuracy statistics provided in Tables IX and X for Guangzhou and Wuhan, three main findings can be summarized. First, the use of all spectral and textural features using both Landsat and ASTER data (All) achieved the best result; the OA indices for Guangzhou and Wuhan based on the RF classifier were 66% and 84%, respectively, which are better than the results with other feature sets. Second, the Landsat data outperformed the ASTER data when only spectral features were used, whether for urban LCZ types or for natural LCZ types. By combining both spectral and textural features, incorporation of the textural features of the ASTER data can achieve a better prediction result than the use of ASTER spectral data alone. However, the improvement seen by adding the textural features of the Landsat data is not significant, possibly due to the relatively lower spatial resolution of the Landsat data. Third, when the performances of different features were compared on the basis of two main LCZ types, including urban types and natural types, it was found that all features performed better in predicting natural types than urban types. In Guangzhou for example, the OA for all results for natural types were above 80%, but the results for all urban types were below 70%, which might indicate that one significant issue of the proposed method is that it still has limitations in differentiating urban LCZ types.

B. Important Features in LCZ Mapping

The Gini importance from the RF classifier is adopted in this study because this index reflects the importance of different features. Based on the Gini importance value, the important spectral and textural features from both Landsat and ASTER data for discriminating different LCZ classes can be determined.

Fig. 5 shows the Gini importance of all features in the generation of LCZ results for both study areas. By fitting a curve with the Gini importance values of all features for both study areas, it is apparent that some spectral and textural features from both ASTER and Landsat data have distinct peak values, such as spectral bands 4 and 5 and textural feature GLCM1 of Landsat data, which indicates that both spectral and textural features from ASTER and Landsat data contribute to the final results.

These features work together to generate the final LCZ results. Compared with both case studies, we found that Wuhan had two dominant features, including bands 7 and 10 of the Landsat data, but Guangzhou achieves five important features, including the spectral bands 1, 5, and 10 and the GLCM mean texture of the Landsat data and band 2 of the ASTER data. This difference might indicate that the situation of Guangzhou is more complex than that of Wuhan for LCZ mapping. Thus, it requires more features to differentiate some LCZ types.

We also note some relatively important spectral features for LCZ mapping of both study areas, like bands 5 and 10 of the Landsat data. These features correspond to the near-infrared, and thermal bands of both sets of satellite data. The importance of these features can be explained by their good representation of the main structures of different LCZ types (e.g., vegetation and thermal emissivity). The importance of the textural features is relatively weaker than that of the above-mentioned spectral features, but some important textural features still might work together to achieve better LCZ mapping results. The relatively important textual features are GLCM mean and dissimilarity textures of different LCZ types. This finding indicates that both textural features from other high-resolution satellite datasets (e.g., sentinel-2) might also be helpful in differentiating some LCZ types in complex urban scenarios.

C. Further Improvements

The proposed approach using Landsat and ASTER data is easy to implement and can achieve promising LCZ mapping results. Our experimental results show that the proposed approach using both datasets could achieve promising LCZ mapping results for both Guangzhou and Wuhan, with OA of 66% and 84%, respectively, which are better than the results from a conventional approach (62% and 81%). These results were consistent with a similar study for Kyiv, Ukraine, in which the OA using Landsat data was 64% [13]. Nevertheless, when the results were assessed for two major LCZ categories, including urban types and natural types, it was found that the overall prediction accuracy for urban types is still unsatisfactory. For Guangzhou, for example, the overall prediction accuracy for urban types was 65%. The OA for urban types for Wuhan (83%) was much better than that for Guangzhou. The main reason might be that Guangzhou is much denser and more complex than Wuhan, which caused the difficulty in differentiating urban types. This result also reflects that high-density urban areas are likely to have low LCZ mapping accuracy. Although the addition of textural information from both Landsat and ASTER data with the proposed approach can improve mapping accuracy, it is still necessary to investigate the addition of more satellite data (e.g., Interference SAR data) to help differentiate complex urban structures, which is vital for high-density and compact cities like Guangzhou.

In addition to the accuracy issue for high-density urban areas, training samples observed from high-resolution imagery have extra errors that might affect the final LCZ mapping result and lower the value of its applications. Given this situation, a standard training database at the continent or country level might

be a solution to eliminate the effects of the training samples for applications with different groups of people.

VII. CONCLUSION

The LCZ classification system provides a standard method to support urban climate studies—UHI analysis. On the one hand, as the input data of some urban climate models, high-quality LCZ mapping result can generate high-quality simulation result. On the other hand, a better LCZ mapping result gives a better understanding of the urban thermal environment, which can benefit in the development of effective migration measures for urban climate issues.

This paper investigated the use of both Landsat and ASTER data in the generation of high-quality LCZ mapping results. Experimental results from two high-density Chinese cities showed that the proposed approach using both spectral and textural information from both Landsat and ASTER data can achieve much better results than the conventional LCZ mapping method using only spectral information from Landsat data. The overall prediction accuracies for Guangzhou and Wuhan were 66% and 84%, respectively, which were better than those of conventional method, which had overall accuracies of 62% and 81%. When comparing Landsat with ASTER data for generating LCZ maps, the Landsat data outperformed the ASTER data because the Landsat data contain much more spectral information than the ASTER data.
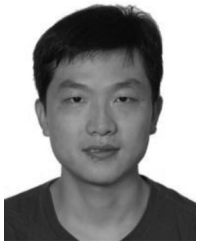
The performance of different features in generating LCZ maps was also compared. It is found that the proposed approach with all features (All) performed the best, followed by the features LT8 + AST, LT8 + GLCM, LT8, AST + GLCM, and, finally, AST. The experimental results confirm that the addition of textural information could actually improve the overall prediction accuracy, especially for urban types. This finding also indicates that the combination of spectral and textural information is vital for the generation of high-quality LCZ mapping results for large, dense cities.

The testing results also show that the OA for urban LCZ types is still a challenging issue. In particular, high-rise highly compact areas had large prediction errors because different urban types in high-density areas are prone to be mixed together. Thus, the addition of building height information (e.g., interference SAR data, or Open Street Map) to differentiate complex urban LCZ types for high-density cities is an important topic for further study.

REFERENCES

[1] A. J. Arnfield, "Two decades of urban climate research: A review of turbulence, exchanges of energy and water, and the urban heat island," *Int. J. Climatol.*, vol. 23, no. 1, pp. 1–26, Jan. 2003.

[2] A. M. Rizwan, L. Y. Dennis, and C. H. Liu, "A review on the generation, determination and mitigation of Urban Heat Island," *J. Environ. Sci.*, vol. 20, no. 1, pp. 120–128, 2008.

[3] I. D. Stewart and T. R. Oke, "Local climate zones for urban temperature studies," *Bull. Amer. Meteorol. Soc.*, vol. 93, no. 12, pp. 1879–1990, Dec. 2012.

[4] P. Gamba, M. Aldrighi, and M. Stasolla, "Robust extraction of urban area extents in HR and VHR SAR images," *IEEE J. Sel. Topics Appl. Earth Observ. Remote Sens.*, vol. 4, no. 1, pp. 27–34, Mar. 2011.

[5] P. Gamba, G. Lisini, P. Liu, P. J. Du, and H. Lin, "Urban climate zone detection and discrimination using object-based analysis of VHR scenes," in *Proc. 4th GEOBIA*, Rio de Janeiro, Brazil, 2012, pp. 70–74.

[6] M. Voltersen, C. Berger, S. Hese, and C. Schmullius, "Object-based land cover mapping and comprehensive feature calculation for an automated derivation of urban structure types at block level," *Remote Sens. Environ.*, vol. 154, pp. 192–201, Nov. 2014.

[7] G. Mills, J. Ching, L. See, and B. Betchel, "An introduction to the WUDAPT project," presented at the 9th Int. Conf. Urban Climate, Toulouse, France, 2015.

[8] B. Bechtel *et al.*, "CENSUS of cities: LCZ classification of cities (Level 0): Workflow and initial results from various cities," presented at the 9th Int. Conf. Urban Climate, Toulouse, France, 2015.

[9] B. Bechtel *et al.*, "Mapping local climate zones for a worldwide database of the form and function of cities," *Int. J. Geograph. Inf.*, vol. 4, no. 1, pp. 199–219, Feb. 2015.

[10] J. Ching, "A perspective on urban canopy layer modeling for weather, climate and air quality applications," *Urban Climate.*, vol. 3, pp. 13–39, May 2013.

[11] J. Feddema, G. Mills, and J. Ching, "Demonstrating the added value of WUDAPT for Urban Climate modelling," presented at the 9th Int. Conf. Urban Climate, Toulouse, France, 2015.

[12] B. Bechtel, L. See, G. Mills, and M. Foley, "Classification of local climate zones using SAR and multispectral data in an arid environment," *IEEE J. Sel. Topics Appl. Earth Observ. Remote Sens.*, vol. xx, no. 9, pp. 1–9, Feb. 2016.

[13] O. Danylo, L. See, B. Bechtel, D. Schepaschenko, and S. Fritz, "Contributing to WUDAPT: A local climate zone classification of two cities in Ukraine," *IEEE J. Sel. Topics Appl. Earth Observ. Remote Sens.*, vol. 9. no. 5, pp. 1841–1853, May 2016.

[14] C. Ren *et al.*, "Local climate zone (LCZ) classification using the world urban database and access portal tools (WUDAPT) method: A case study in Wuhan and Hangzhou," presented at the 4th Int. Conf. Countermeasure Urban Heat Islands, Singapore, 2016.

[15] C. Ren *et al.*, "The accuracy of LCZ maps generated by the world urban database and access portal tools (WUDAPT) method: A case study of Hong Kong," presented at the 4th Int. Conf. Countermeasure Urban Heat Islands, Singapore, 2016.

[16] M. Cai, C. Ren, Y. Xu, W. Dai, and X. M. Wang, "Local climate zone study for sustainable megacities development by using improved WUDAPT methodology—A case study in Guangzhou," presented at the Int. Conf. Geograph. Health Living Cities: Making Cities Healthy for All (H-City), Hong Kong, 2016.

[17] I. D. Stewart, "A systematic review and scientific critique of methodology in modern urban heat island literature," *Int. J. Climatol.*, vol. 31, no. 2, pp. 200–217, Feb. 2011.

[18] T. J. Chandler, "London's urban climate," *Geograph. J.*, vol. 128, no. 3, pp. 279–298, Sep. 1962.

[19] R. Ellefsen, "Mapping and measuring buildings in the canopy boundary layer in ten U.S. cities," *Energy Buildings*, vol. 16, no. 3–4. pp. 1025–1049, 1991.

[20] B. Bechtel and C. Daneke, "Classification of local climate zones based on multiple earth observation data," *IEEE J. Sel. Topics Appl. Earth Observ. Remote Sens.*, vol. 5, no. 4, pp. 1191–1202, Aug. 2012.

[21] Q. H. Weng, "Fractal analysis of satellite-detected urban heat island effect," *Photogramm. Eng. Remote Sens.*, vol. 69, no. 5, pp. 555–566, May 2003.

[22] Q. H, Weng and S. Yang, "Urban air pollution patterns, land use, and thermal landscape: An examination of the linkage using GIS," *Environ. Monit. Assess.*, vol. 117, no. 1, pp. 463–489, Jun. 2006.

[23] J. Q. Zhang and Y. P. Wang, "Study of the relationships between the spatial extent of surface urban heat islands and urban characteristic factors based on Landsat ETM+ data," *Sensors*, vol. 8, no. 11, pp. 7453–7468, Nov. 2008.

[24] G. Y. Ren, Z. Y. Chu, Z .H. Chen, and Y. Y. Ren, "Implications of temporal change in urban heat island intensity observed at Beijing and Wuhan stations," *Geophys. Res. Lett.*, vol. 34, no. 5, pp. 1–5, Mar. 2007.

[25] K. Li and Y. Zhang, "Comparative and combinative study of urban heat island in Wuhan City with remote sensing and CFD simulation," *Sensors*, vol. 8, no. 10, pp. 6692–6703, Oct. 2008.

[26] J. R.G. Pontius and M. Millones, "Death to Kappa: Birth of quantity disagreement and allocation disagreement for accuracy assessment," *Int. J. Remote Sens.*, vol. 32, no. 15, pp. 4407–4429, Aug. 2011.

This article has been accepted for inclusion in a future issue of this journal. Content is final as presented, with the exception of pagination.

XU *et al.*: CLASSIFICATION OF LOCAL CLIMATE ZONES USING ASTER AND LANDSAT DATA FOR HIGH-DENSITY CITIES

9

Yong Xu received the B.S. degree in surveying engineering and the M.S. degree in photogrammetry from Hohai University, Nanjing, China, in 2005 and 2008 respectively, and the Ph.D. degree in geography from the Chinese Unviersity of Hong Kong, Hong Kong, China, in 2012.

He is currently a Postdoctoral Fellow with the Institue of Future Cities, The Chinese University of Hong Kong. His current research interests include remote sensing, GIS, spatial analysis, and their applications in urban climate studies.

Dr. Xu is a Reviewer for numerous international journals, like IEEE GRSL and IEEE JSTARS.

Ng Yan Yung Edward received the B.Sc. degree in Architecture & Environmental Design from the University of Nottingham, Nottinghamshire, UK, in 1983, the M.Sc. degree in Architecture from the University of Manchester, Manchester, UK, in 1986, and the Ph.D. degree in Architecture from the University of Cambridge, Cambridge, UK, in 1991. He is currently a Professor of Architecture in the School of Architecture, The Chinese University of Hong Kong (CUHK), Hong Kong, China.

He was an Architect before becoming a Professor. He specializes in Green Building, Environmental and Sustainable Design, and Urban Climatology for City Planning. At CUHK, he is also the Director of the Master of Science of Sustainable and Environmental Design Programme. As an environmental consultant to the Government of the Hong Kong Special Administrative Region, he developed the performance-based daylight design practice note, the Air Ventilation Assessment Technical Guidelines and the Urban Climatic Maps for City Planning.
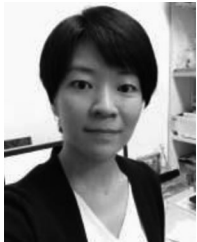
Chao Ren received the B.Sc. degree in Architecture from Xi'an Jiaotong University, Xi'an, China, in 2005, and the Ph.D degree in Architecture from the Chinese University of Hong Kong, Hong Kong, China, in 2010. She is currently an Associate Professor in the School of Architecture, The Chinese University of Hong Kong (CUHK), Hong Kong, China. Her current research interests include sustainable urban and environmental design and urban climatic application in urban planning. She is the Programme Manager of the M.Sc. Sustainable and Environmental Design Programme at CUHK and. She has involved in several governmental research projects, such as "(Hong Kong) Urban Climatic Map and Standards for Wind Environment—Feasibility Study," "Eco-Planning for Kaohsiung, Taiwan by Using Urban Climatic Map," "Macau Urban Climatic Map Study," and EU–Interreg IVB-project titled "Future Cities—Urban Networks to Face Climate Change."

Prof. Ren a registered BEAM Professional.

Tianjun Wu received the B.S. degree in mathematics and information science and the M.S. degree in applied mathematics from Chang'an University, Xi'an, China, in 2009 and 2012 respectively, and the Ph.D. degree in cartography and geographical information system from the State Key Laboratory of Remote Sensing Sciences, Institute of Remote Sensing and Digital Earth (RADI), Chinese Academy of Sciences, Beijing, China, in 2015.

He is currently a Lecturer in the Department of Mathematics and Information Science, College of Science, Chang'an University. His current research interests include geocomputation, remote sensing image processing, and information analysis.
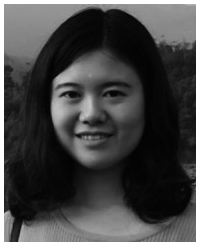
Meng Cai received the Master's degree in geoinformation science from the Chinese University of Hong Kong, Hong Kong, China, in 2014.

She is currently a Research Assistant with the Institue of Future Cities, The Chinese University of Hong Kong. She is involved in GIS and remote sensing. Her current research interests include urban morphology and its impact on urban environment, remote sensing applications in urban climate studies, and heatwave health risk mapping.